Measurement of the complete core plasma flow across the LOC-SOC transition at ASDEX Upgrade

A. Lebschy[1,2], R. M. McDermott[1], C. Angioni[1], B. Geiger[1], D. Prisiazhniuk[1,2], M. Cavedon[1], G. D. Conway[1], R. Dux[1], M. G. Dunne[1], A. Kappatou[1], T. Pütterich[1], U. Stroth[1,2], E. Viezzer[3,1] and the ASDEX Upgrade Team

[1]Max-Planck-Institut für Plasmaphysik, Boltzmannstr. 2, D-85748 Garching, Germany
[2]Physik-Department E28, Technische Universität München, D-85748 Garching, Germany
[3]Dpt. of Atomic, Molecular and Nuclear Physics, University of Seville, Avda. Reina Mercedes, 41012 Seville, Spain

E-mail: alexander.lebschy@ipp.mpg.de

Abstract. A newly installed core charge exchange recombination spectroscopy (CXRS) diagnostic at ASDEX Upgrade (AUG) enables the evaluation of the core poloidal rotation (u_{pol}) through the inboard-outboard asymmetry of the toroidal rotation with an accuracy of 0.5 to 1 km/s. Using this technique, the total plasma flow has been measured in Ohmic L-mode plasmas across the transition from the linear to saturated ohmic confinement (LOC-SOC) regimes. The core poloidal rotation of the plasma around mid-radius is found to be always in the ion diamagnetic direction, in disagreement with neoclassical (NC) predictions. The edge rotation is found to be electron-directed and consistent with NC codes. This measurement provides as well the missing ingredient to evaluate the core $\vec{E} \times \vec{B}$ velocity ($u_{\vec{E}\times\vec{B}}$) from data only, which can then be compared to measurements of the perpendicular velocity of the turbulent fluctuations ($u_{\perp}$) to gain information on the turbulent phase velocity (v_{ph}). The non neoclassical u_{pol} from CXRS leads to good agreement between $u_{\vec{E}\times\vec{B}}$ and $u_{\perp}$ indicating that v_{ph} is small and at similar values as found with gyrokinetic simulations. Moreover, the data shows a shift of v_{ph} in the ion-diamagnetic direction at the edge after the transition from LOC to SOC consistent with a change in the dominant turbulence regime. The upgrade of the core CXRS system provides as well a deeper insight into the intrinsic rotation. This paper shows that the reversal of the core toroidal rotation occurs clearly after the LOC-SOC transition and concomitant with the peaking of the electron density.

Submitted to: *Nucl. Fusion*

1. Introduction

It was found in the early 70's that the global energy confinement time (τ_{E}) scales linearly with the electron density (n_{e}) [1–4]. A few years later, however, a saturation of τ_{E} above a certain critical density was observed at the ISX-A tokamak [5]. In subsequent years, this behavior was confirmed at various devices like Alcator-C [6], Doublet III [7], and ASDEX [8]. Today, this result is ubiquitous to Ohmically heated tokamak plasmas [9–15] and the critical density divides the Ohmic confinement into two regimes: the linear Ohmic confinement (LOC) and the saturated Ohmic confinement (SOC) regime. One example of a LOC-SOC transition is shown in figure 1 for the ASDEX Upgrade (AUG) tokamak. The energy confinement time in LOC is compared to the neo-Alcator scaling [16] (purple squares) and in SOC to the ITER89-P L-mode scaling [17] (blue diamonds). While the ITER89-P L-mode scaling matches the experimentally measured values perfectly, the neo-Alcator scaling under-predicts the experimental values; this behavior was already observed in [15] and is related to the shape of present day tokamaks. In order to have an accurate determination of the critical density at the LOC-SOC transition, the experimental values of τ_{E} are fitted with a two-line fit (red line in figure 1) meaning that the lines above and below the critical density as well as the crossing point is determined numerically. This method of identifying the LOC-SOC transition is used for all discharges shown in this work.

For many years, a commonly accepted theoretical explanation for the transition from LOC to SOC was a change in the dominant transport from trapped electron modes (TEM) in LOC to ion temperature gradient (ITG) turbulence in SOC [5, 7, 11, 13, 18]. The increase of τ_{E} in LOC is then attributed to the de-trapping of trapped electrons leading to a decrease of the thermal diffusivity and an improved coupling between electrons and ions. Due to the lower ion temperature gradient and thermal diffusivity, the ions confine the energy better. At the LOC-SOC transition, the thermal diffusivity of electrons and ions become independent of the electron density and the energy transport is covered by the ions [11]. It has to be mentioned that the transition is not a sudden phenomena occurring at all radial points in the plasma. It is rather a gradual transition moving from the edge to the core of the plasma [19] and modeling work from AUG [20] and Alcator-C Mod [21] even indicate that the the transition is only occurring at the edge of the plasma and ITG is the dominant turbulent mode

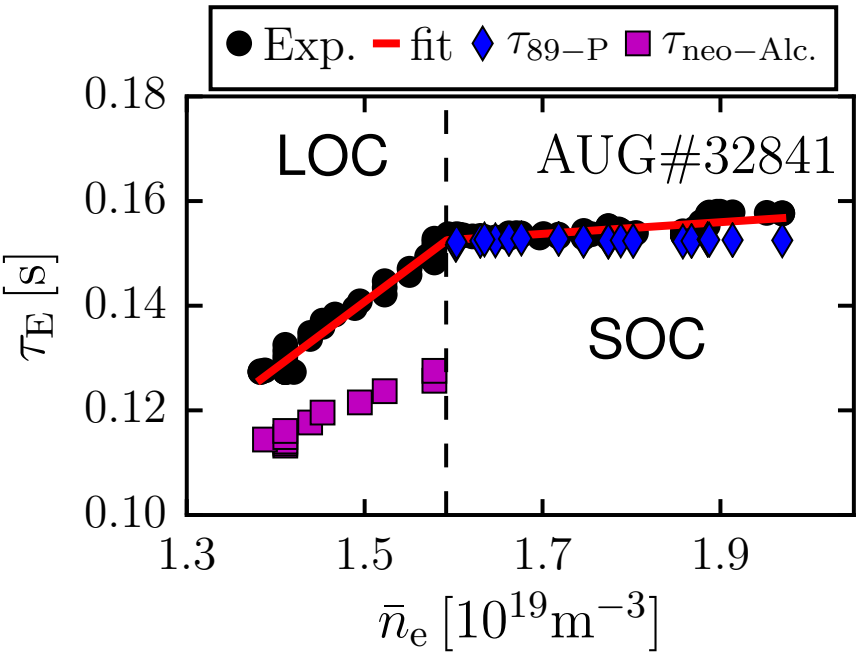

Figure 1. τ_E (black circles) is calculated from the thermal energies of electrons and ions and shown as a function of the averaged electron density measured via laser interferometry. The neo-Alcator scaling (purple squares) [16] underpredicts the observed confinement times in the LOC regime and the ITER89-P L-mode scaling [17] (blue diamonds) for the SOC regime has an excellent agreement with the measured τ_E values. A two-line fit (red line) has been used in order to determine the density at the LOC-SOC transition (dashed line).

inside $\rho_{pol} < 0.8$. Gyrokinetic simulations done at AUG [20] suggest that the LOC-SOC transition is not determined by a change from TEM to ITG. It is rather the ion energy transport that gets stronger at higher densities due to the decreasing dilution of the plasma with increasing density and the strongly stiff ion transport that leads to a saturation of τ_E. The TEM to ITG transition is, however, necessary to explain the observation of the electron density peaking seen in a the parameter regime of the LOC-SOC transition [18]. In this case, we would not necessarily expect to see a change in v_{ph} correlated with the LOC-SOC transition, but rather after the maximum peaking of the electron density profile.

A significant amount of experimental work has been done supporting the presence of TEM in LOC and the suppression of TEM turbulence in SOC [19, 21–24, and references therein]. Additionally, ITG turbulence was detected in other experiments in the SOC regime at multiple devices [10,13,14,25,26, and references therein]. While

much of the performed analysis is qualitatively consistent with a transition from TEM to ITG across the LOC-SOC transition, a change via direct measurements was not actually demonstrated or measurements deep in the LOC and deep in the SOC were compared such that no statement on the point of the transition could be done.

In this paper, we extend previous investigations from [27] to gain direct information on the dominant type of turbulence present in the LOC and the SOC regimes. Due to the upgrade of the core charge exchange recombination spectroscopy (CXRS) diagnostics at AUG, it is possible to determine the core poloidal rotation (u_{pol}) from the inboard-outboard asymmetry of the toroidal rotation (u_{tor}) [28, 29]. This enables the possibility to study the complete flow on a flux surface and a comparison to neoclassical predictions. In addition, this measurement provides the missing ingredient to calculate the $\vec{E} \times \vec{B}$ velocity ($u_{\vec{E}\times\vec{B}}$) in the plasma core from data only and, therefore, to measure the turbulent phase velocity (v_{ph}) via comparisons with the perpendicular velocity ($u_{\perp}$) from reflectometry measurements [30, 31]:

$$u_{\perp}(\vec{k}) = u_{\vec{E}\times\vec{B}} + v_{\mathrm{ph}}(\vec{k}). \tag{1}$$

The turbulent phase velocity and perpendicular velocity depend, in general, on the wave number $\vec{k}$ of the observed fluctuations. Detailed comparisons of reflectometry measurements at different wave numbers reveal, however, the same $u_{\perp}$ within the uncertainty of the measurement showing that the dependence on $\vec{k}$ in equation (1) can be neglected [32]. The phase velocity is directed in the electron diamagnetic direction for TEM and in the ion diamagnetic direction for ITG turbulence and v_{ph} is, therefore, indicative of the dominant turbulent mode and a change in the sign of v_{ph} would be expected assuming that there is a change from TEM to ITG.

The structure of this paper is as follows: section 2 presents detailed information about the diagnostics used and the techniques applied to get information on u_{pol} and v_{ph}. Section 3 shows the evolution of the experimental and neoclassical (NC) u_{pol} across the LOC-SOC transition. In section 4, a detailed comparison between reflectometry and CXRS measurements is shown and calculations of v_{ph} from gyrokinetic simulations are presented. Subsequently, the observed momentum changes that accompany the LOC-SOC transition are discussed in more depth in section 5. Section 6 is dedicated to the discussion and the summary of the observed results.

2. Measurement technique

One way to gain additional information on the type of turbulence present in tokamak plasmas is to measure the turbulent phase velocity. At AUG, there are various reflectometry systems [31,32] measuring $u_\perp$ of density fluctuations, which is connected to $v_{\rm ph}$ and $u_{\vec{E}\times\vec{B}}$ via equation (1). The phase velocity of the turbulence is, however, expected to be smaller than $u_{\vec{E}\times\vec{B}}$; such that accurate measurements of both $u_{\vec{E}\times\vec{B}}$ and $u_\perp$ are necessary to gain information on $v_{\rm ph}$.

For this work, the Poloidal Correlation Reflectometry (PCR) system is of special interest. This diagnostic measures the density fluctuations with a set of five antennas arranged toroidally and poloidally and is sensitive to wavenumbers in the range of 0 to $3\,\mathrm{cm}^{-1}$. The correlation of the signals from the different antennas gives then the magnetic pitch angle and $u_\perp$ [32].

In order to evaluate the $u_{\vec{E}\times\vec{B}} = E_{\rm r}/B$ velocity of the plasma, the radial electric field $E_{\rm r}$ is calculated via the radial force balance equation:

$$E_{\rm r} = \frac{\nabla p_\alpha}{e\, Z_\alpha\, n_\alpha} - u_{{\rm pol},\alpha}\, B_{\rm tor} + u_{{\rm tor},\alpha}\, B_{\rm pol} \tag{2}$$

where Z_α is the charge number, $p_\alpha = n_\alpha\, T_\alpha$ is the plasma pressure, given by the product of density n_α and temperature T_α, $u_{{\rm pol},\alpha}$ is the poloidal rotation, and $u_{{\rm tor},\alpha}$ is the toroidal rotation for the plasma species α. $B_{\rm tor}$ and $B_{\rm pol}$ are the toroidal and poloidal magnetic field components obtained from the magnetic equilibrium reconstruction.

A common technique to measure the temperature T_α, density n_α and $u_{{\rm tor},\alpha}$ of low-Z impurities is charge exchange recombination spectroscopy [33]. This technique can be used as well to measure $u_{{\rm pol},\alpha}$ in the steep pedestal region, i.e. for values of the normalized poloidal flux coordinate $\rho_{\rm pol} > 0.95$. In the core, however, direct measurements of $u_{{\rm pol},\alpha}$ are challenging due to small velocities present there, a low signal-to-noise ratio due to the attenuation of the injected beam and complicated atomic physic's effects [34, 35]. Through the evaluation of the inboard-outboard asymmetry of the toroidal rotation it is, however, possible to get an indirect measurement of the core $u_{{\rm pol},\alpha}$ with an accuracy better than $1\,\mathrm{km/s}$. Note that the index α will not be marked explicitly in the following and all CXRS profiles shown here correspond to profiles from the fully stripped B^{5+} population.

Any plasma flow, for which the divergence free condition $\nabla(n\,\vec{u}) = 0$ holds, can

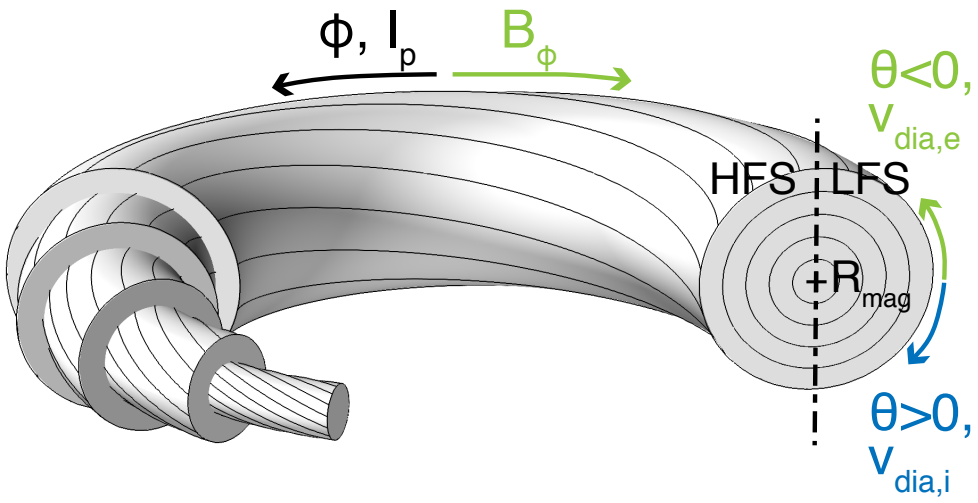

Figure 2. Illustration of the AUG coordinate system and indication of the electron diamagnetic direction ($v_{\mathrm{dia,e}}$) and ion diamagnetic direction ($v_{\mathrm{dia,i}}$) with respect to the poloidal angle θ. Additionally, the toroidal angle ϕ is depicted and correspondingly the direction of the plasma current and the toroidal magnetic field. This figure shows as well the high-field-side (HFS) and low-field-side (LFS) of the plasma and the location of the magnetic axis (R_{mag}, indicated with a +).

be expressed through a component parallel to the magnetic field and a rigid body toroidal rotation allowing the following equation to be applied even for non neoclassical situations [36]:

$$\vec{u} = \hat{u}(\psi)\,\vec{B} + \hat{\omega}(\psi)\,R\,\vec{e}_{\mathrm{tor}}, \tag{3}$$

where $\vec{B}$ is the magnetic field, R the major radius, and $\vec{e}_{\mathrm{tor}}$ the unity vector in the toroidal direction. Equation (3) implies that the two flux functions $\hat{\omega}(\psi)$ and $\hat{u}(\psi)$ can be reconstructed from two measurements on the same flux surface, which provides the measurement of the full plasma flow and, therefore, also u_{pol}. This method was first implemented at the PDX tokamak [37] and has been established recently at TCV [38] and DIII-D [39]. For the special case that there is no poloidal rotation, the flux function $\hat{u}$ would be zero and the toroidal plasma flow can be expressed with a rigid body rotation, i.e. the inboard- and outboard-side of the plasma rotates toroidally

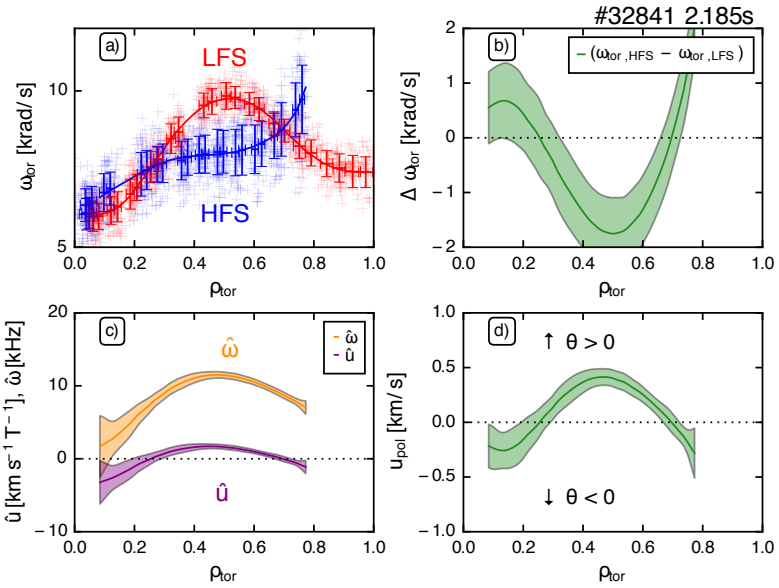

Figure 3. Illustration of the indirect u_{pol} reconstruction technique. Through measurements of (a) the toroidal rotation frequency $\omega_{\mathrm{tor}} = u_{\mathrm{tor}}/R$ on both, the LFS and HFS, (b) the difference $\Delta\,\omega_{\mathrm{tor}}$ can be calculated giving (c) the flux functions $\hat{\omega}(\psi)$ and $\hat{u}(\psi)$ of the general plasma flow - see equation (3). Multiplying $\hat{u}(\psi)$ with the local poloidal magnetic field results, finally, in (d) a value for u_{pol} at the LFS mid-plane. Positive values correspond to downwards rotations on the LFS mid-plane ($\theta > 0$) and negative ones to upwards rotations ($\theta < 0$).

with the same rotation frequency $\omega_{\mathrm{tor}} = u_{\mathrm{tor}}/R$.

To guarantee a good disentanglement of the rigid body rotation from the component parallel to the magnetic field, the radial distance between the two points on the same flux surface should be large. Therefore, the upgrades to the core CXRS system at AUG [28] were designed to enable measurements on the low-field side (LFS, where $R > R_{\mathrm{mag}}$) and high-field side (HFS, where $R < R_{\mathrm{mag}}$) of the plasma such that measurements of T, n and u_{tor} across the full plasma width are now available. R_{mag} refers to the magnetic axis and is depicted in figure 2. This enables measurements of u_{pol} with an accuracy of 0.5 to 1.0 km/s depending on parameters and the impurity content of the plasma [29].

The standard AUG coordinate system (see figure 2) is a right-handed one with the minor radius r, the poloidal angle θ, and the toroidal angle ϕ. From a top-down view of the machine, ϕ is positive in the counter-clockwise direction, which corresponds to the co-current direction for all of the experiments shown here. The toroidal magnetic field is in the clockwise direction such that it is negative in the used coordinate system.

Viewing the poloidal cross-section of AUG, θ is positive in the clockwise direction, i.e. vertically downward at the LFS mid-plane. In terms of drift directions, a flow in the $+\theta$ direction corresponds to a drift in the ion diamagnetic direction and a flow in the $-\theta$ direction to a drift in the electron diamagnetic direction for all plasma discharges shown in this work.

Figure 3 illustrates the indirect reconstruction method of the poloidal rotation. Panel a shows that the toroidal rotation frequencies on the LFS and the HFS do not agree implying that there is a poloidal rotation according to equation (3). The connected flux function $\hat{u}(\psi)$ can be calculated according to [38]:

$$\hat{u}(\psi) = s_\mathrm{b}\, F^{-1}\left(\frac{\omega_\mathrm{tor,HFS} - \omega_\mathrm{tor,LFS}}{R_\mathrm{HFS}^{-2} - R_\mathrm{LFS}^{-2}}\right), \tag{4}$$

where $s_\mathrm{b} = \mathrm{sign}(B_\mathrm{tor})$ accounts for the direction of the toroidal magnetic field with respect to the toroidal direction and is defined such that $F = |R\, B_\mathrm{tor}| \geq 0$. Panel c shows the reconstructed flux functions $\hat{\omega}(\psi)$ and $\hat{u}(\psi)$. Compared to $\Delta\,\omega_\mathrm{tor}$, $\hat{u}(\psi)$ is flipped horizontally since the toroidal magnetic field points in a different direction than the toroidal direction, i.e. $s_\mathrm{b} = -1$. From equation (3) it can be seen that by knowing the magnetic field structure, u_pol can be calculated via the projection of the general plasma flow in the poloidal direction:

$$u_\mathrm{pol} = s_\mathrm{j}\, \hat{u}(\psi)\, B_\mathrm{pol}, \tag{5}$$

where s_j accounts for the direction of plasma current in terms of the poloidal angle. The poloidal rotation profile at the LFS mid-plane ($\theta = 0$) is shown in figure 3d as a function of ρ_tor for the fully stripped B^{5+} ion with its direction specified in terms of the poloidal angle θ. The normalized toroidal flux coordinate ρ_tor at a certain position x in the plasma is defined via the toroidal flux Ψ at the position, at the magnetic axis, and at the separatrix, i.e. the last closed flux surface:

$$\rho_\mathrm{tor} = \sqrt{\frac{\Psi_\mathrm{axis} - \Psi_\mathrm{x}}{\Psi_\mathrm{x} - \Psi_\mathrm{separatrix}}}. \tag{6}$$

From figure 3a and d it can be seen that the poloidal plasma flow is in the ion/electron diamagnetic direction when ω_tor is smaller/larger on the HFS compared to the LFS.

The error bars on the profiles are calculated with a Monte-Carlo approach. The individual measurements (red and blue crosses in figure 3a) are varied with a 2–D Gaussian distribution according to the radial error (x-axis) resulting from the finite resolution of CXRS system and the measurement uncertainty (y-axis) resulting from

the fitting of the CXRS spectra. The known errors are used as the standard deviation σ of a Gauss distribution and there are typically 1000 variations used to generate a set of artificial data that are within the uncertainty of the measurement. Each of these variations (see light blue and red crosses in figure 3a) gives a new toroidal rotation frequency and a new u_{pol} profile. The final u_{pol} profile is calculated as the mean from all of these variations and the error is given by the standard deviation of the individual variations from the mean value. A more detailed description of this technique can be found in the appendix of [38]. Here it has to be noted that in order to compare the LFS and HFS ω_{tor} values on the same flux surface, a magnetic equilibrium is needed to map the real space coordinates of the measurements to the normalized toroidal flux coordinate ρ_{tor}. Inevitably, the magnetic equilibrium used has some uncertainties, which are larger for higher pressure discharges with high fast ion fractions (not the case in Ohmic L-mode plasmas) and for low q_{95} discharges. The equilibria used for these discharges are based on the measurements of magnetic pick-up coils and the estimation of the $q = 1$ surface from sawtooth crashes. If asymmetries in the LFS-HFS ion temperature profile are observed, i.e. the measurements do not overlay as a function of ρ_{tor}, the HFS T_{i} and u_{tor} profiles are shifted accordingly in order to avoid equilibrium effects on the reconstruction of u_{pol}. This method has been introduced in [40] and the applied shifts are within the uncertainty of the pickup coil measurements [28]. Additionally, possible atomic physics effects are carefully treated for the reconstruction of the core poloidal rotation. The charge exchange cross section effect resulting from angles between the lines-of-sight (LOSs) geometry of the CXRS system and the injection trajectory of the NBI source in combination with the energy dependence of the charge exchange cross section is corrected using an approach similar to Hellermann *et al.* [41] presented in [28]. A set of lookup tables using a range of ion temperatures and toroidal rotations has been created such that the measured temperatures and rotations can be corrected routinely. For Ohmic L-mode discharges, these corrections are typically on the order of 1 km/s [28]. Gyro-orbit effects [34] leading to an apparent poloidal rotation are neglected since all of the LOSs are almost parallel to the magnetic field lines [28].

In order to obtain CXRS measurements in Ohmically heated L-mode plasmas, a combination of fast CXRS measurement (4 ms) and short neutral beam injection (NBI) blips (12–16 ms) is used [42]. Typically, there are 3–4 measured spectra during

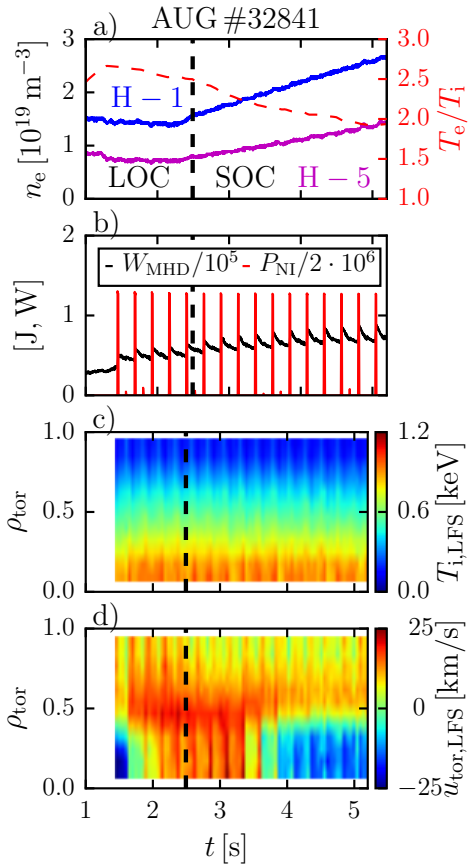

Figure 4. From top to bottom: time evolution of (a) the electron density for one core (blue, H–1) and edge (magenta, H–5) channel of the laser interferometry diagnostic as well as T_e/T_i in the plasma core at $\rho_{tor} = 0.1$ (dashed red line), (b) the plasma stored energy (W_{MHD}) in black and the NBI blips in red, (c) a contour plot of the ion temperature and (d) the toroidal rotation for a low density L-mode plasma with a density ramp. Note, that CXRS diagnostic is only capable of measuring during the injection of NBI blips. The values for T_i and u_{tor} in between are, therefore, interpolated in the contour plot. The point of the LOC-SOC transition is marked with a dashed black line.

one beam blip such that the evolution in the profile can be taken into account. To do this, each of these four measurements is fitted with a spline function and the profile before the beam blip is determined by using a linear backward extrapolation. With this method, an impact of the neutral beam blip on the plasma, if any, can be approximately removed. As seen from figure 4b, the beam blip leads to an increase in the plasma stored energy W_{MHD} and, therefore, the beam blips are only injected every 240 ms so that W_{MHD} can decay back to its original values before the next beam blip comes. This can be seen very well between the second and fourth beam blip in

figure 4b, in a phase of constant density. Later in the discharge, the density of the plasma is increase from beam blip to beam blip and, therefore, the stored energy of the plasma is increased as well. The timing between the blips is chosen such that it is 1.5 to 2 times the energy confinement implying that the impact of the NBI source should be removed by the next blip since the momentum confinement time is similar to the energy confinement time [43–45].

The impurity density profile is also required for the evaluation of the radial electric field. It is calculated via the measured CXRS intensities and knowledge of the number of neutral particles injected during the beam blip. Unfortunately, as the geometry of the injected neutral beam is not well known during such short blips, it is not possible to use standard neutral attenuation codes to determine the number of neutral particles. Instead, measurements of the populations of the atomic state $n = 3$ of the different beam energy components are made via beam emission spectroscopy [46] along parallel lines of sight and with identical time resolution. These populations are then converted to the ground and first excited state ($n = 1$ and $n = 2$) populations using a collisional radiative model and used to calculate the neutral particle distribution of the heating beam which is necessary to evaluate the impurity density profiles from the intensity of the measured active CXRS line.

3. Measurement of the poloidal rotation across the LOC-SOC transition

Figure 4 shows the time evolution of a plasma discharge performed for this work. Since the LOC-SOC transition is defined by a critical density, the density in each discharge was intentionally increased with a feedback gas puff algorithm (see figure 4a) to transition the plasmas from the LOC into the SOC regime. Thereby, the coupling between electrons and ions increased and $T_\mathrm{e}/T_\mathrm{i}$ decreased at higher n_e values. The LOC-SOC transition for the discharges shown in figures 1 and 4 (600 kA, -2.4 T) occurs at a density of $1.6 \cdot 10^{19}\,\mathrm{m}^{-3}$ at 2.5 s as marked with a vertical dashed black line in figure 4. Figure 4c and d show the measured T_i and u_tor values on the LFS as contour plots where the x-axis corresponds to time, the y-axis to the radial position in the normalized toroidal flux coordinate, and the color coding to the measured temperatures and rotations. It can be seen that while the ion temperature profile stays unchanged throughout the plasma discharge, there is an interesting phenomenon

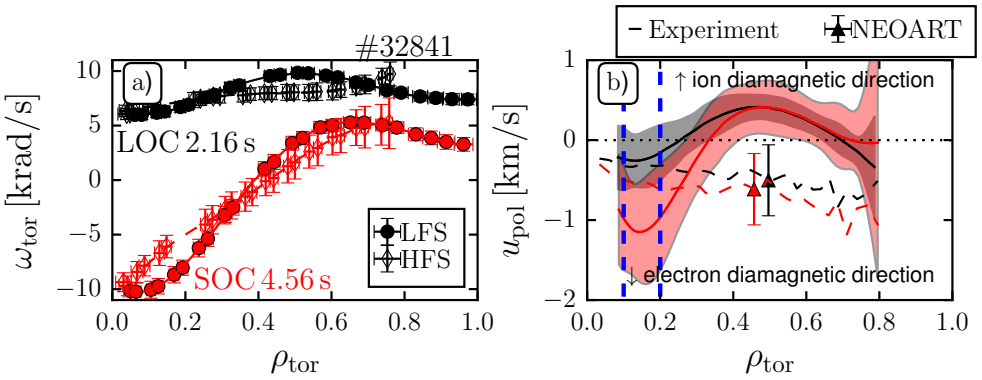

Figure 5. (a) Measured LFS (filled circles) and HFS (open diamonds) ω_{tor} profiles and (b) comparison of the measured u_{pol} profile (solid lines) with the neoclassical predictions (dashed lines) from NEOART for a time point in the LOC (black) and the SOC (red). The dashed blue lines indicate two out of 10 radial intervals used for the poloidal rotation database shown in figure 6.

observed with the toroidal rotation: The plasma starts off with a counter-current toroidal rotation (i.e. negative), switches then to a co-current phase at roughly 2 s, and goes back counter-current at 3.5 s. These changes of u_{tor} will be the topic of section 5. In total, four discharges of this kind were performed for this work with plasma currents of 0.6 MA (# 32841), 0.8 MA (# 32842, # 32843), and 1.0 MA (# 32844).

Figure 5a and 5b show, respectively, the measured ω_{tor} profile and the reconstructed poloidal rotation during the LOC (black) and SOC (red) phases of discharge # 32841. In addition, the neoclassical predictions of u_{pol} from NEOART [47] are shown in figure 5b with dashed lines and the same color coding. It has to be mentioned here that the experimentally measured poloidal rotation and the neoclassical predictions correspond to the fully stripped boron impurity, and not the main ion species. It can be seen that both the experimental (solid lines) and neoclassical (dashed lines) poloidal rotations are unchanged across the transition from LOC to SOC. Especially for the experimental values it is impressive since the toroidal rotation changes quite significantly, which shows the sensitivity of this technique. The neoclassical prediction is always in the electron diamagnetic direction and ranges from -1 km/s at the plasma edge to -0.5 km/s in the plasma core. Note that 'edge' here refers to the outermost measurement positions of the core CXRS system, but does not include the edge pedestal region. The experimental poloidal rotation, on the other hand, is in the electron diamagnetic direction only for $\rho_{tor} > 0.7$ and $\rho_{tor} < 0.3$. In these regions, the NC predictions and experimentally measured values for u_{pol}

agree within their uncertainties. In between, however, u_{pol} is directed in the ion diamagnetic direction and, therefore, non neoclassical. This observation is similar to measurements of the core poloidal rotation in low torque NBI heated plasmas at DIII-D [48] and goes in the direction of previous observations at AUG where non neoclassical poloidal rotations were necessary to explain differences between CXRS and reflectometry measurements [27]. Additionally, non neoclassical poloidal rotations have been found at DIII-D [49] and in internal transport barriers in JET [50, 51]. While the results from JET show poloidal rotations in the same direction as from NC theory, those from AUG and DIII-D show different drift directions compared to theory. The results from AUG differ from previous direct measurements at TEXT [52], MAST [53], and NSTX [54] and previous indirect measurements at TCV [38] that show neoclassical poloidal rotations from the plasma core to the plasma edge. The measured non neoclassical poloidal rotation implies that there is some other mechanism at work in these low density Ohmic L-mode plasmas to explain the difference between the NC prediction and experimentally measured poloidal rotation. The poloidal rotation of the impurities is caused by friction with the main ions. A non neoclassical u_{pol} of the impurity ions would, therefore, also imply a non neoclassical poloidal rotation of the main ions. CXRS measurements of the main ion rotation were unfortunately not available in these discharges.

In order to study the general behavior of the experimentally measured poloidal rotations and the NC predictions relative to the LOC-SOC transition, a database approach was chosen and the relevant quantities ($u_{\mathrm{pol,exp}}$, $u_{\mathrm{pol,NC}}$, and the time of the LOC-SOC transition t_{LS}) were determined for the four discharges used in this work. Figure 6 shows the neoclassical u_{pol} versus the experimental values for four different time intervals with respect to the LOC-SOC transition: $t - t_{\mathrm{LS}} \in [-1\,\mathrm{s}, -0.5\,\mathrm{s}]$, $[-0.5\,\mathrm{s}, 0\,\mathrm{s}]$, $[0\,\mathrm{s}, 0.5\,\mathrm{s}]$ and $[0.5\,\mathrm{s}, 1\,\mathrm{s}]$. The times of the LOC-SOC transition were determined as discussed in section 1. This figure includes data from four discharges, comprising a scan of the plasma current from 0.6 to 1.0 MA. A positive sign corresponds to a flow in the ion diamagnetic direction and a negative one to a flow in the electron diamagnetic direction (consistent with the sign convention in figure 5).

Each data point in figure 6 corresponds to a single beam blip in a discharge and an average over a fixed radial interval. For this, the normalized toroidal flux

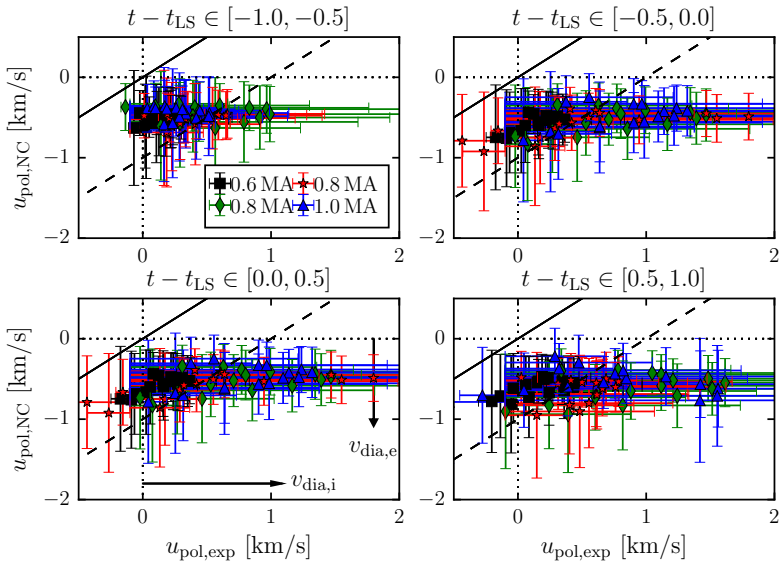

Figure 6. Comparison of the experimentally measured poloidal rotation to the neoclassical prediction from NEOART for different time intervals relative to the LOC-SOC transition. The solid line corresponds to the 1–1 line, i.e. a perfect agreement between measurement and theory. Additionally, a $\pm 1\,\mathrm{km/s}$ deviation from theory is shown with a dashed line.

coordinate ρ_{tor} is used and the data is binned into intervals with a width $\Delta\rho_{\mathrm{tor}} = 0.1$ (see blue dashed vertical lines in figure 5b). In these intervals, the measured profiles are averaged and the error bars presented in figure 6 correspond to a combination of the statistical error from the averaging, errors in the magnetic equilibrium and the calculated measurement errors. With this approach, the measured data can be clustered and compared for multiple shots. The radial region for the points in figure 6 is constrained to $0.3 < \rho_{\mathrm{tor}} < 0.7$. Note that this is the region that shows the discrepancy between the measurement and the neoclassical theory. The lower boundary is due to the error bars on the plasma current distribution and, therefore, on the poloidal magnetic field, which become quite large for positions closer to the magnetic axis. The outer boundary is set by the availability of CXRS measurements on both the LFS and HFS of the plasma, see figure 3.

It can be seen that the neoclassical u_{pol} profiles are in a range from -1 to $-0.5\,\mathrm{km/s}$. They are always directed in the electron diamagnetic direction and the profiles shown in figure 5b are a good representation of the general behavior of the NC predictions. The reconstructed values from NEOART have been compared as

well to reconstructions from NCLASS [55] and NEO [56] which give the same profiles for the NC poloidal rotation. It is not surprising that there is only a small change in the theoretical predictions since the neoclassical u_{pol} depends on the gradients in the plasma profiles and the LOC-SOC transition is occurring in a small window such that there is as well only a moderate change in the plasma profiles. For the experimental reconstructions, the range is a bit broader (from slightly negative values up to $+1.5\,\mathrm{km/s}$). For the plasma discharges at 0.8 MA and 1.0 MA, there seems to be a small spin-up of the poloidal rotation when going from LOC to SOC. This increase is, however, not outside of the error bars of the measurement such that no clear statement can be made. For all discharges and all time points a clear shift of the experimentally measured poloidal rotation in the ion diamagnetic direction is observed, i.e. the data points are shifted to the right from the 1–1 line (solid black line), which would correspond to a perfect agreement of measurement and NC prediction. The dashed black line corresponds to a deviation between experiment and theory of $\pm\,1\,\mathrm{km/s}$. The increasing uncertainties in the experimental values with time relative to the LOC-SOC transition results from increasing error bars of the HFS CXRS profiles at higher collisionalities.

From the experimentally observed dependencies it may be possible to infer some information on the mechanisms at work driving this non neoclassical poloidal rotation. The parameter range explored in these Ohmic L-mode plasmas is relatively narrow and, moreover, the plasma parameters are highly correlated making correlation analysis of the measurements impractical. Within this dataset a weak dependency was found on the collisionality meaning that the differences between experiment and theory are larger for smaller collisionalities. This dataset is, however, insufficient to draw firm conclusions. The scaling of the experimental poloidal rotation with theoretically relevant parameters will be the topic of future publications.

4. Measurement of the phase velocity across the LOC-SOC transition

The knowledge of the impurity poloidal rotation enables the experimental measurement of the radial electric field in the plasma core according to equation (2) and, therefore, the evaluation of $u_{\vec{E}\times\vec{B}}$. The solid lines in figure 7 correspond to the calculated $u_{\vec{E}\times\vec{B}}$ from CXRS for one time point in the LOC (black) and one time

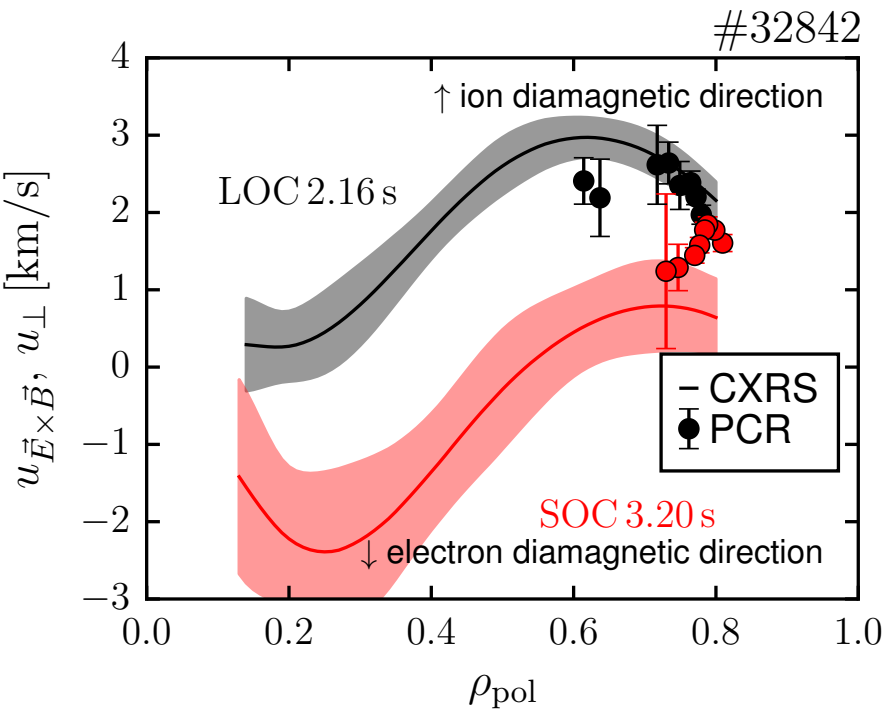

Figure 7. Comparison of the u_{ExB} measurement from CXRS (solid line) to poloidal correlation reflectometry data of $u_\perp$ (dots) for both confinement regimes, the LOC (black) and the SOC (red).

point in the SOC (red) for the plasma discharge # 32842. This figure does not show a comparison to NC theory since the measured temperature, density, and toroidal rotation profiles are taken to evaluate the NC $u_{\vec{E}\times\vec{B}}$ such that the only difference in $u_{\vec{E}\times\vec{B}}$ between theory and measurement is u_{pol}. It was shown in the previous section that the measured poloidal rotation is more in the ion diamagnetic direction than the NC values and, therefore, one would see the same behavior in figure 7, i.e. the neoclassical prediction would lie below the experimental $u_{\vec{E}\times\vec{B}}$. Instead, figure 7 shows a comparison with the perpendicular propagation velocity of the turbulence as measured by the PCR diagnostic (filled circles). The difference between the two data sets gives the turbulent phase velocity according to equation (1). If $u_\perp$ is larger than u_{ExB}, v_{ph} is in the ion diamagnetic direction and if $u_\perp$ is smaller than u_{ExB} then v_{ph} is in the electron diamagnetic direction. The comparison shows that the measured values of $u_{\vec{E}\times\vec{B}}$ from CXRS and $u_\perp$ from PCR is close in both the LOC and in the SOC regime. Thus, v_{ph} is small and the observed changes in the phase velocity are

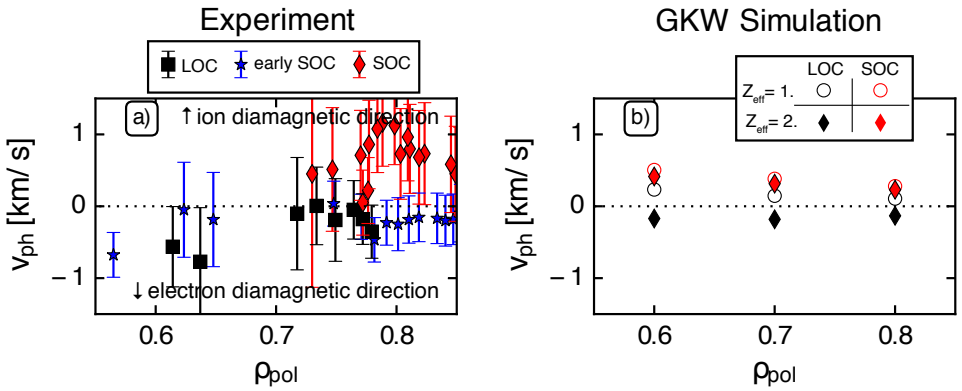

Figure 8. Comparison of (a) the experimentally measured turbulent phase velocities obtained by the subtraction of the perpendicular velocities and the ExB velocities in LOC (black) and SOC (red) to (b) gyrokinetic simulations of $v_{\rm ph}$ for two different impurity content levels.

smaller than 1 km/s in both the LOC and the SOC, which is close to the resolution boundary of the combined analysis of both diagnostics.

For the described dataset of LOC-SOC discharges, there were four time points where the reflectometry and the CXRS had data of sufficient quality for the comparison. Figure 8a shows the turbulent phase velocity evaluation for the four time points resulting from two different LOC-SOC transitions, discharges # 32841 and # 32842. From discharge # 32841, the profiles at 2.65 s and 5.0 s were used for the comparison. The first time point corresponds to 150 ms after the LOC-SOC transition (which will be called *early SOC* in the following), while the second point is deep in the SOC regime. From discharge # 32842, the profiles at 2.16 s and 3.20 s were taken (see as well figure 7), where the first corresponds to a measurement in the LOC and the second to a measurement deep in the SOC. From the experimental data it can be seen that there is no change of the turbulent phase velocity across the LOC-SOC transition for density fluctuations with a perpendicular wave number $k_\perp = 0$–$3\,{\rm cm}^{-1}$ measured with the PCR diagnostic, i.e. the measured phase velocity in LOC and in early SOC are very similar with small values below 1 km/s in the electron diamagnetic direction. The observed size scale corresponds to typical TEM/ITG size scales. Later on, deep in the SOC regime, a systematic increase of $v_{\rm ph}$ is observed between $0.7 < \rho_{\rm pol} < 0.9$ in the ion diamagnetic direction. The observations are consistent with the idea that the saturation of the energy confinement time is not directly connected to a change

in the dominant turbulence regime. Instead, there is a change of the turbulent phase velocity from electron to ion directed at the edge of the plasma indicating a change of the dominant turbulent mode from TEM to ITG in this region at some point in the SOC regime. While it is possible to track the full evolution of u_{tor}, u_{pol} and $u_{\vec{E}\times\vec{B}}$ from the CXRS measurements across the LOC-SOC transitions, it is not possible to follow the full evolution of v_{ph} from this dataset and the exact point of the change from electron diamagnetic direction to ion diamagnetic direction cannot be determined although it is clear that this change happens in the SOC regime. The change of v_{ph} is, therefore, not correlated with the LOC-SOC transition itself. Additionally, no information on the evolution at smaller radii is available from this data due to a lack of reflectometry measurements at these locations.

Figure 8b shows, additionally, gyrokinetic predictions of v_{ph} from the nonlinear gyro-kinetic flux tube code GKW [57]. These phase velocities are calculated for the most unstable mode for the same wavelength number at which the PCR diagnostic is measuring. In order to test the stability of the turbulent modes, the GKW simulations have been performed for different $Z_{\mathrm{eff}} = \sum n_{\mathrm{i}} Z_{\mathrm{i}}^2/n_{\mathrm{e}}$ values. $Z_{\mathrm{eff}} = 1$ corresponds to a pure deuterium plasma and $Z_{\mathrm{eff}} = 2$ to a boron concentration of 5 %. Due to the increasing density when going from LOC to SOC, the impurity content decreases such that the Z_{eff} is higher in LOC than in SOC. Z_{eff} can be measured from the bremsstrahlung background, active CXRS measurements, or estimations of the loop voltage since the plasma conductivity depends on the effective charge. These estimations show a decrease of Z_{eff} from approximately 2 in the LOC to 1.2 in the SOC. Therefore, the GKW predictions for $Z_{\mathrm{eff}} = 2$ should be used when comparing with the measured data in the LOC (black diamonds) and $Z_{\mathrm{eff}} = 1$ (open red circles) in the SOC. The results from the GKW code show a similar behavior as the measurements of the phase velocity. The absolute change in v_{ph} is roughly a factor of 2 higher in the experiment compared to the simulations. However, they agree within the uncertainties of the experimental data. From figure 8b it can be seen that the direction of the phase velocity (that is the dominant mode) is sensitive to the impurity content of the plasma. The main effect of an increased impurity content is the dilution of the main ions leading to a reduction of the ITG growth rate and a broadening of the domain of dominant TEM instabilities.

5. Reversal of the core toroidal rotation

Ohmic L-mode discharges feature another interesting phenomenon: the intrinsic core toroidal is observed to spontaneously reverse from the co- to the counter-current direction when the electron density is increased. In this paper, intrinsic rotation refers to the toroidal rotation of the plasma established in the absence of externally applied torque. The rotation reversal was observed first at TCV [58] and since then also at Alcator C-Mod [59], AUG [27, 60], KSTAR [61], and MAST [62] and is in-line with AUG Doppler reflectometry measurements across the LOC-SOC transition [63].

In [27, 60] the behavior of the intrinsic rotation was observed in AUG for a large number of Ohmic L-mode plasmas. The rotation measurements in this database, however, were made with CXRS diagnostics with lower light throughput and lower radial resolution than the diagnostics presented in section 2. As a result, the uncertainties on the measured profiles were often several km/s, which is 2 to 3 times larger than what is achievable with the newly installed CXRS diagnostics. Moreover, the previous analysis relied heavily on the electron density profiles measurements, which have been significantly improved since the time these measurements were made. These facts motivated a revisit of the intrinsic rotation in Ohmic L-mode discharges and a comparison to the previous analysis and results.

Figure 9a shows the evolution of the rotation gradient $u^{'} = -(R^2/v_{\mathrm{thi,i}})\,\mathrm{d}\,\omega/\mathrm{d}r$ at a radial position of $\rho_{\mathrm{tor}} = 0.65$. Here, $v_{\mathrm{thi,i}}$ is the main ion thermal velocity $v_{\mathrm{thi,i}} = \sqrt{2\,T_{\mathrm{i}}/m_{\mathrm{i}}}$. Additionally, the Mach number M and the normalized logarithmic electron density gradient length $R/L_{n_{\mathrm{e}}} = R\,(\nabla_r n_{\mathrm{e}})/n_{\mathrm{e}}$ are shown in panels b and c. All quantities are shown as a function of the effective collisionality ν_{eff} which is evaluated according to:

$$\nu_{\mathrm{eff}} = 0.00279 \cdot \left(15.94 - 0.5\,\log\frac{n_{\mathrm{e}}}{T_{\mathrm{e}}}\right) \cdot \frac{n_{\mathrm{e}}}{T_{\mathrm{e}}^2}\,R\,\sqrt{m_{\mathrm{A}}}\,Z_{\mathrm{eff}}, \tag{7}$$

where the electron density is given in $10^{19}\,\mathrm{m}^{-3}$, T_{e} in keV, R in m, and the mass of the main ion species m_{A} in amu, i.e. $m_{\mathrm{A}} = 2$. The beginning of the discharges which feature counter-current directed toroidal rotation are intentionally omitted in this figure. This phase is transient and cannot be maintained by holding all controlled plasma variables constant. However, it is worth noting that these data points also show the same dominant parameter trends as observed in the plasma flat top under steady conditions, namely $R/L_{n_{\mathrm{e}}}$ and ν_{eff}. The dependency on $R/L_{T_{\mathrm{e}}}$ and $R/L_{T_{\mathrm{i}}}$ is

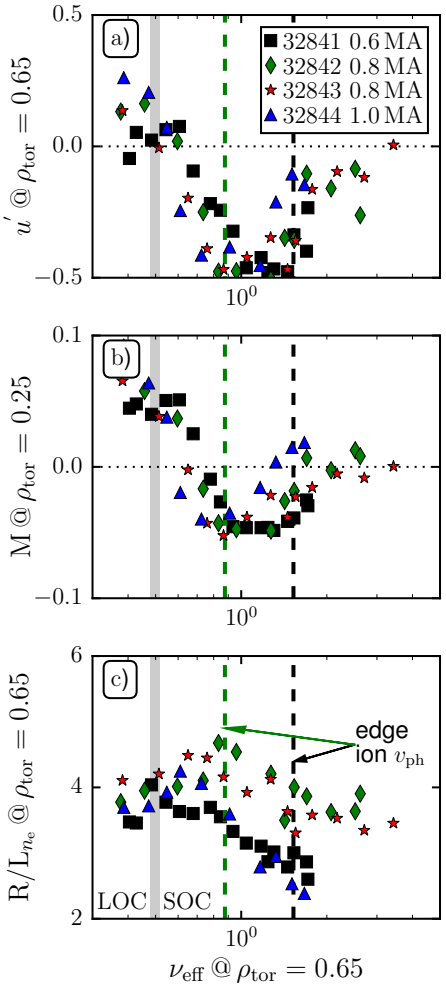

Figure 9. Evolution of the rotation gradient (a), Mach number (b), and normalized gradient length of the electron density (c) as a function of effective collisionality for four different plasma discharges at different plasma currents (0.6 MA: 32841 with black squares; 0.8 MA: 32842 with green diamonds, 32843 with red stars; and 1.0 MA: 32844 with blue triangles) at the radial position $\rho_{\mathrm{tor}} = 0.65$. The LOC-SOC transitions for the different discharges are marked with a gray area. The vertical dashed lines correspond to the collisionalities at which phase velocities in the ion diamagnetic direction were measured.

observed to be weaker than previously observed [64].

Similar to previous work, the effective collisionality is a good variable to describe the data. In this parametrization, the different densities of the LOC-SOC transition and the rotation reversal collapse to one. In contrast to the previous work, however, there is a clear time delay between the reversal of the core toroidal rotation and the

LOC-SOC transition (see figure 9b). The electron density peaking in figure 9c is as well less pronounced compared to previous work. However, a strong correlation between these parameters is still observed consistent with previous results.

To illustrate the sequence of events observed in these plasmas the collisionalities at which phase velocities in the ion diamagnetic direction are measured are additionally shown in figure 9 with vertically dashed lines. Here one can see that as the collisionality is increased first a LOC-SOC transition is observed, which is a global phenomenon in the energy confinement time. Subsequently, the core toroidal rotation reverses from the co- to the counter-current direction concomitant with an increase in R/L_{n_e}. Finally, phase velocities in the ion diamagnetic direction are measured in the edge region of the plasma. The peaking of the electron density profile at mid-radius is expected to happen while the dominant turbulence mode at this location is still TEM, but near the TEM-ITG transition [65]. The edge measurements at this time point indicate that there is already an ion-directed turbulence propagation, which supports previous indications that the transition occurs first at the plasma edge and then propagates inwards [19].

6. Summary

Due to an upgrade of the core CXRS systems, an accurate measurement of the core impurity poloidal rotation at ASDEX Upgrade is possible. Measurements in Ohmic L-mode discharges show that it is directed in the ion diamagnetic direction at mid-radius, which is in the opposite direction as predicted from neoclassical theory. These non neoclassical rotations help to explain previous comparisons of CXRS and Doppler reflectometry data at AUG [27]. The poloidal rotation switches sign outside of $\rho_{\mathrm{tor}} > 0.7$ and reaches similar values as predicted from NC theory.

The indirect measurement of the impurity poloidal rotation in the plasma core is, furthermore, the missing ingredient to evaluate the core $\vec{E} \times \vec{B}$ velocity. The comparison of this quantity with turbulence propagation measurements of the perpendicular velocity enables an evaluation of the turbulent phase velocity at different points in the LOC-SOC evolution. An increase in the ion diamagnetic direction is observed at the plasma edge ($\rho_{\mathrm{pol}} > 0.8$) consistent with a change in the plasma turbulence towards a more ITG dominated regime in this region. The gathered data

suggests that the change in v_{ph} is not connected to the LOC-SOC transition, but occurs at some point in the SOC regime.

The upgrade of the core CXRS systems provided, additionally, a significant reduction of the error bars for the intrinsic rotation measurement and lead to new insights compared to previous observations. Compared to previous work, similar dominant parameters for the rotation reversal were found, i.e. $R/L_{n_{\mathrm{e}}}$ and ν_{eff}. With the availability of v_{ph} measurements in theses discharge it was possible to experimentally measure the sequence of events in these Ohmic L-mode discharges. The gathered data suggests that there first the LOC-SOC transition, which is followed by a change in the direction of the core intrinsic toroidal rotation from co- to counter-current direction. The core rotation change is accompanied by a peaking of the core electron density and lastly the edge phase velocity changes sign.

Acknowledgments

The authors are very grateful for the fruitful discussions with I. Erofeev, E. Fable and F. Ryter. We thankfully acknowledge the financial support from the Helmholtz Association of German Research Centers through the Helmholtz Young Investigators Group program. This work has been carried out within the framework of the EUROfusion Consortium and has received funding from the Euratom research and training program 2014-2018 under grant agreement No 633053. The views and opinions expressed herein do not necessarily reflect those of the European Commission.

Bibliography

[1] E. P. Gorbunov, S. V. Mirnov, and V. S. Strelkov. Energy confinement time of a plasma as a function of the discharge parameters in TOKAMAK-3. *Nuclear Fusion*, 10(1):43, 1970.

[2] C. Daughney. Empirical scaling for present Ohmically heated tokamaks. *Nuclear Fusion*, 15(6):967, 1975.

[3] D. L. Jassby, D. R. Cohn, and R. R. Parker. Reply to "Comments on the paper 'Characteristics of high-density tokamak ignition reactors'". *Nuclear Fusion*, 16(6):1045, 1976.

[4] W. Pfeiffer and R. E. Waltz. Empirical scaling laws for energy confinement in Ohmically-heated tokamaks. *Nuclear Fusion*, 19(1):51, 1979.

[5] M. Murakami, G. H. Neilson, H. C. Howe, T. C. Jernigan, S. C. Bates, C. E. Bush, R. J. Colchin, J. L. Dunlap, P. H. Edmonds, K. W. Hill, R. C. Isler, H. E. Ketterer, P. W. King, D. W. McNeill, J. T. Mihalczo, R. V. Neidigh, V. K. Pare, M. J. Saltmarsh, J. B. Wilgen, and

B. Zurro. Plasma confinement studies in the ISX-A tokamak. *Phys. Rev. Lett.*, 42:655–658, Mar 1979.

[6] S. Fairfax, A. Gondhalekar, R. Granetz, M. Greenwald, and D. Gwinn. Energy and particle confinement in the Alcator tokamaks. In Brussels International Atomic Energy Agency, editor, *Proceedings of the Eigth International Conference on Plasma Physics and Controlled Nuclear Fusion Research*, volume 1, pages 439–450, 1980.

[7] S. Ejima, T. W. Petrie, A. C. Riviere, T. R. Angel, C. J. Armentrout, D. R. Baker, F. P. Blau, G. Bramson, N. H. Brooks, R. W. Callis, R. P. Chase, J. C. DeBoo, J. S. DeGrassie, E. S. Fairbanks, R. K. Fisher, R. J. Groebner, C. L. Hsieh, J. Hugill, G. L. Jahns, J. M. Lohr, J. L. Luxon, M.A. Mahdavi, F. B. Marcus, N. Ohyabu, P. I. Petersen, W. W. Pfeiffer, R. P. Seraydarian, A. M. Sleeper, R. T. Snider, R. D. Stambaugh, T. Tamano, T. S. Taylor, R. E. Waltz, J. C. Wesley, and S. S. Wojtowicz. Scaling of energy confinement with minor radius, current and density in doublet III Ohmically heated plasmas. *Nuclear Fusion*, 22(12):1627, 1982.

[8] E. E. Simmet and the ASDEX Team. Statistical analysis of the global energy confinement time in Ohmic discharges in the ASDEX tokamak. *Plasma Physics and Controlled Fusion*, 38(5):689, 1996.

[9] R. R. Parker, M. Greenwald, S. C. Luckhardt, E. S. Marmar, M. Porkolab, and S. M. Wolfe. Progress in tokamak research at MIT. *Nuclear Fusion*, 25(9):1127, 1985.

[10] X. Garbet, J. Payan, C. Laviron, P. Devynck, S. K. Saha, H. Capes, X. P. Chen, J. P. Coulon, C. Gil, G. R. Harris, T. Hutter, A.-L. Pecquet, A. Truc, P. Hennequin, F. Gervais, and A. Quemeneur. Turbulence and energy confinement in TORE SUPRA Ohmic discharges. *Nuclear Fusion*, 32(12):2147, 1992.

[11] Ulrich Stroth. A comparative study of transport in stellarators and tokamaks. *Plasma Physics and Controlled Fusion*, 40(1):9, 1998.

[12] G. Bracco and K. Thomsen. Analysis of a global energy confinement database for JET Ohmic plasmas. *Nuclear Fusion*, 37(6):759, 1997.

[13] C. L. Rettig, T. L. Rhodes, J. N. Leboeuf, W. A. Peebles, E. J. Doyle, G. M. Staebler, K. H. Burrell, and R. A. Moyer. Search for the ion temperature gradient mode in a tokamak plasma and comparison with theoretical predictions. *Physics of Plasmas*, 8(5):2232–2237, 2001.

[14] B. Esposito, M. Marinucci, M. Romanelli, G. Bracco, C. Castaldo, V. Cocilovo, E. Giovannozzi, M. Leigheb, G. Monari, S. Nowak, C. Sozzi, O. Tudisco, R. Cesario, D. Frigione, C. Gormezano, G. Granucci, L. Panaccione, V. Pericoli-Ridolfini, L. Pieroni, FTU team, and ECRH team. Transport analysis of Ohmic, L-mode and improved confinement discharges in FTU. *Plasma Physics and Controlled Fusion*, 46(11):1793, 2004.

[15] J. E. Rice, M. J. Greenwald, Y. A. Podpaly, M. L. Reinke, P. H. Diamond, J. W. Hughes, N. T. Howard, Y. Ma, I. Cziegler, B. P. Duval, P. C. Ennever, D. Ernst, C. L. Fiore, C. Gao, J. H. Irby, E. S. Marmar, M. Porkolab, N. Tsujii, and S. M. Wolfe. Ohmic energy confinement saturation and core toroidal rotation reversal in Alcator C-Mod plasmas. *Physics of Plasmas*, 19(5):056106, 2012.

[16] R. J. Goldston. Energy confinement scaling in tokamaks: some implications of recent

experiments with Ohmic and strong auxiliary heating. *Plasma Physics and Controlled Fusion*, 26(1A):87, 1984.

[17] P. N. Yushmanov, T. Takizuka, K. S. Riedel, O. J. W. F. Kardaun, J. G. Cordey, S. M. Kaye, and D. E. Post. Scalings for tokamak energy confinement. *Nuclear Fusion*, 30(10):1999, 1990.

[18] C. Angioni, A. G. Peeters, F. Ryter, F. Jenko, G. D. Conway, T. Dannert, H. U. Fahrbach, M. Reich, W. Suttrop, ASDEX Upgrade Team, and L. Fattorini. Relationship between density peaking, particle thermodiffusion, Ohmic confinement, and microinstabilities in ASDEX Upgrade L-mode plasmas. *Physics of Plasmas*, 12(4):040701, 2005.

[19] F. Ryter, C. Angioni, A. G. Peeters, F. Leuterer, H.-U. Fahrbach, and W. Suttrop. Experimental study of Trapped-Electron-Mode properties in tokamaks: threshold and stabilization by collisions. *Phys. Rev. Lett.*, 95:085001, Aug 2005.

[20] I. Erofeev, E. Fable, C. Angioni, R. M. McDermott, and the ASDEX Upgrade Team. Theorybased modeling of LOCSOC transitions in ASDEX Upgrade. *Nuclear Fusion*, "submitted to NF" 2017.

[21] C. Sung, A. E. White, N. T. Howard, C. Y. Oi, J. E. Rice, C. Gao, P. Ennever, M. Porkolab, F. Parra, D. Mikkelsen, D. Ernst, J. Walk, J. W. Hughes, J. Irby, C. Kasten, A. E. Hubbard, M. J. Greenwald, and the Alcator C-Mod Team. Changes in core electron temperature fluctuations across the Ohmic energy confinement transition in Alcator C-Mod plasmas. *Nuclear Fusion*, 53(8):083010, 2013.

[22] H. Arnichand, R. Sabot, S. Hacquin, A. Krämer-Flecken, X. Garbet, J. Citrin, C. Bourdelle, G. Hornung, J. Bernardo, C. Bottereau, F. Clairet, G. Falchetto, and J. C. Giacalone. Quasi-coherent modes and electron-driven turbulence. *Nuclear Fusion*, 54(12):123017, 2014.

[23] H. Arnichand, J. Citrin, S. Hacquin, R. Sabot, A. Krämer-Flecken, X. Garbet, C. Bourdelle, C. Bottereau, F. Clairet, J. C. Giacalone, Z. O. Guimaraes-Filho, R. Guirlet, G. Hornung, A. Lebschy, P. Lotte, P. Maget, A. Medvedeva, D. Molina, V. Nikolaeva, D. Prisiazhniuk, the Tore Supra, and the ASDEX Upgrade teams. Identification of trapped electron modes in frequency fluctuation spectra. *Plasma Physics and Controlled Fusion*, 58(1):014037, 2016.

[24] D. Prisiazhniuk, A. Krämer-Flecken, G. D. Conway, A. Lebschy, C. Angioni, T. Happel, U. Stroth, P. Manz, and the ASDEX Upgrade Team. Characterization of the turbulence during loc-soc transition using poloidal correlation reflectometry at asdex upgrade. In P. Mantica, G. Giruzzi, M. Fajardo, T. Gans, S. Poedts, and Geneva) N. Vennekens (European Physical Society, editors, *Europhysics Conference Abstracts (CD-ROM, Proc. of the 43th EPS Conference on Plasma Physics, Leuven, Belgium, 2016)*, volume 40A (2016), 2016.

[25] D. L. Brower, W. A. Peebles, S. K. Kim, N. C. Luhmann, W. M. Tang, and P. E. Phillips. Observation of a high-density ion mode in tokamak microturbulence. *Phys. Rev. Lett.*, 59:48–51, Jul 1987.

[26] L. Lin, E. M. Edlund, M. Porkolab, Y. Lin, and S. J. Wukitch. Vertical localization of phase contrast imaging diagnostic in Alcator C-Mod. *Review of Scientific Instruments*, 77(10):10E918, 2006.

[27] R. M. McDermott, C. Angioni, G. D. Conway, R. Dux, E. Fable, R. Fischer, T. Pütterich,

F. Ryter, E. Viezzer, and the ASDEX Upgrade Team. Core intrinsic rotation behaviour in ASDEX Upgrade Ohmic L-mode plasmas. *Nuclear Fusion*, 54(4):043009, 2014.

[28] R. M. McDermott, A. Lebschy, B. Geiger, C. Bruhn, M. Cavedon, R. Dux, A. Kappatou, T. Pütterich, E. Viezzer, and the ASDEX Upgrade Team. Extensions to the core charge exchange recombination diagnostic suite at asdex upgrade. *Review of Scientific Instruments*, 88:073508, 2017.

[29] A. Lebschy, R. M. McDermott, B. Geiger, M. Cavedon, M. G. Dunne, R. Dux, R. Fischer, E. Viezzer, and the ASDEX Upgrade team. Indirect measurement of the poloidal rotation in the core of ASDEX Upgrade plasmas with charge exchange recombination spectroscopy. In R. Bingham, Suttrop, S. Atzeni, R. Foest, K. McClements, B. Goncalves, C. Silva, and Geneva) R. Coelho (European Physical Society, editors, *Europhysics Conference Abstracts (CD-ROM, Proc. of the 42th EPS Conference on Plasma Physics, Lisbon, Portugal, 2015)*, volume 39E (2015), 2015.

[30] M. Hirsch, E. Holzhauer, J. Baldzuhn, B. Kurzan, and B. Scott. Doppler reflectometry for the investigation of propagating density perturbations. *Plasma Physics and Controlled Fusion*, 43(12):1641, 2001.

[31] G. D. Conway, J. Schirmer, S. Klenge, W. Suttrop, E. Holzhauer, and the ASDEX Upgrade Team. Plasma rotation profile measurements using Doppler reflectometry. *Plasma Physics and Controlled Fusion*, 46(6):951, 2004.

[32] D. Prisiazhniuk, A. Krämer-Flecken, G. D. Conway, T. Happel, A. Lebschy, P. Manz, V. Nikolaeva, U. Stroth, and the ASDEX Upgrade Team. Magnetic field pitch angle and perpendicular velocity measurements from multi-point time-delay estimation of poloidal correlation reflectometry. *Plasma Physics and Controlled Fusion*, 59(2):025013, 2017.

[33] R. J. Fonck, D. S. Darrow, and K. P. Jaehnig. Determination of plasma-ion velocity distribution via charge-exchange recombination spectroscopy. *Phys. Rev. A*, 29:3288–3309, Jun 1984.

[34] R. E. Bell and E. J. Synakowski. New understanding of poloidal rotation measurements in a tokamak plasma. *AIP Conference Proceedings*, 547(1):39–52, 2000.

[35] W. M. Solomon, K. H. Burrell, P. Gohil, R. J. Groebner, and L. R. Baylor. Extraction of poloidal velocity from charge exchange recombination spectroscopy measurements. *Review of Scientific Instruments*, 75(10):3481–3486, 2004.

[36] F. L. Hinton and R. D. Hazeltine. Theory of plasma transport in toroidal confinement systems. *Rev. Mod. Phys.*, 48:239–308, Apr 1976.

[37] K. Brau, M. Bitter, R.J. Goldston, D. Manos, K. McGuire, and S. Suckewer. Plasma rotation in the PDX tokamak. *Nuclear Fusion*, 23(12):1643, 1983.

[38] A. Bortolon, Y. Camenen, A.N. Karpushov, B.P. Duval, Y. Andrebe, L. Federspiel, O. Sauter, and the TCV Team. Indirect measurement of poloidal rotation using inboard-outboard asymmetry of toroidal rotation and comparison with neoclassical predictions. *Nuclear Fusion*, 53(2):023002, 2013.

[39] C. Chrystal, K. H. Burrell, B. A. Grierson, R. J. Groebner, and D. H. Kaplan. Calculation of impurity poloidal rotation from measured poloidal asymmetries in the toroidal rotation of a tokamak plasma. *Review of Scientific Instruments*, 83(10):10D501, 2012.

[40] C. Chrystal, K. H. Burrell, B. A. Grierson, G. M. Staebler, W. M. Solomon, W. X. Wang, T. L. Rhodes, L. Schmitz, J. E. Kinsey, L. L. Lao, J. S. deGrassie, S. Mordijck, and O. Meneghini. Testing neoclassical and turbulent effects on poloidal rotation in the core of DIII-D. *Physics of Plasmas*, 21(7):072504, 2014.

[41] M. von Hellermann, P. Breger, J. Frieling, R. Konig, W. Mandl, A. Maas, and H. P. Summers. Analytical approximation of cross-section effects on charge exchange spectra observed in hot fusion plasmas. *Plasma Physics and Controlled Fusion*, 37(2):71, 1995.

[42] R. M. McDermott, C. Angioni, R. Dux, E. Fable, T. Pütterich, F. Ryter, A. Salmi, T. Tala, G. Tardini, E. Viezzer, and the ASDEX Upgrade Team. Core momentum and particle transport studies in the ASDEX Upgrade tokamak. *Plasma Physics and Controlled Fusion*, 53(12):124013, 2011.

[43] A. Kallenbach, H. M. Mayer, G. Fussmann, V. Mertens, U. Stroth, O. Vollmer, and the ASDEX Team. Characterization of the angular momentum transport in ASDEX. *Plasma Physics and Controlled Fusion*, 33(6):595, 1991.

[44] K.-D. Zastrow, W. G. F. Core, L.-G. Eriksson, M. G. Von Hellermann, A. C. Howman, and R. W. T. König. Transfer rates of toroidal angular momentum during neutral beam injection. *Nuclear Fusion*, 38(2):257, 1998.

[45] J. S. deGrassie, D. R. Baker, K. H. Burrell, P. Gohil, C. M. Greenfield, R. J. Groebner, and D. M. Thomas. Toroidal rotation in neutral beam heated discharges in DIII-D. *Nuclear Fusion*, 43(2):142, 2003.

[46] R. M. Dux, B. Geiger, R. M. McDermott, L. Menchero, T. P̈terich, E. Viezzer, and ASDEX Upgrade Team. Impurity density determination using charge exchange and beam emission spectroscopy at ASDEX Upgrade. In S. Ratynskaya, L. Blomberg, and Geneva) A. Fasoli (European Physical Society, editors, *Europhysics Conference Abstracts (CD-ROM, Proc. of the 39th EPS Conference on Plasma Physics, Stockholm, Sweden, 2012)*, volume 36F (2012), 2012.

[47] A. G. Peeters. Reduced charge state equations that describe pfirsch schlueter impurity transport in tokamak plasma. *Physics of Plasmas*, 7(1):268–275, 2000.

[48] B. A. Grierson, K. H. Burrell, W. M. Solomon, R. V. Budny, and J. Candy. Collisionality scaling of main-ion toroidal and poloidal rotation in low torque DIII-D plasmas. *Nuclear Fusion*, 53(6):063010, 2013.

[49] W. M. Solomon, K. H. Burrell, R. Andre, L. R. Baylor, R. Budny, P. Gohil, R. J. Groebner, C. T. Holcomb, W. A. Houlberg, and M. R. Wade. Experimental test of the neoclassical theory of impurity poloidal rotation in tokamaks. *Physics of Plasmas*, 13(5):056116, 2006.

[50] K. Crombé, Y. Andrew, M. Brix, C. Giroud, S. Hacquin, N. C. Hawkes, A. Murari, M. F. F. Nave, J. Ongena, V. Parail, G. Van Oost, I. Voitsekhovitch, and K.-D. Zastrow. Poloidal rotation dynamics, radial electric field, and neoclassical theory in the jet internal-transport-barrier region. *Phys. Rev. Lett.*, 95:155003, Oct 2005.

[51] T. Tala, Y. Andrew, K. Crombé, P.C. de Vries, X. Garbet, N. Hawkes, H. Nordman, K. Rantamäki, P. Strand, A. Thyagaraja, J. Weiland, E. Asp, Y. Baranov, C. Challis, G. Corrigan, A. Eriksson, C. Giroud, M.-D. Hua, I. Jenkins, H.C.M. Knoops, X. Litaudon,

P. Mantica, V. Naulin, V. Parail, K.-D. Zastrow, and JET-EFDA contributors. Toroidal and poloidal momentum transport studies in JET. *Nuclear Fusion*, 47(8):1012, 2007.

[52] A. G. Meigs and William L. Rowan. Impurity poloidal rotation velocity in tokamaks. *Physics of Plasmas*, 1(4):960–967, 1994.

[53] A. R. Field, J. McCone, N. J. Conway, M. Dunstan, S. Newton, and M. Wisse. Comparison of measured poloidal rotation in mast spherical tokamak plasmas with neo-classical predictions. *Plasma Physics and Controlled Fusion*, 51(10):105002, 2009.

[54] R. E. Bell, R. Andre, S. M. Kaye, R. A. Kolesnikov, B. P. LeBlanc, G. Rewoldt, W. X. Wang, and S. A. Sabbagh. Comparison of poloidal velocity measurements to neoclassical theory on the national spherical torus experimenta). *Physics of Plasmas*, 17(8):082507, 2010.

[55] W. A. Houlberg, K. C. Shaing, S. P. Hirshman, and M. C. Zarnstorff. Bootstrap current and neoclassical transport in tokamaks of arbitrary collisionality and aspect ratio. *Physics of Plasmas*, 4(9):3230–3242, 1997.

[56] E A Belli and J Candy. Kinetic calculation of neoclassical transport including self-consistent electron and impurity dynamics. *Plasma Physics and Controlled Fusion*, 50(9):095010, 2008.

[57] A. G. Peeters, Y. Camenen, F. J. Casson, W. A. Hornsby, A. P. Snodin, D. Strintzi, and G. Szepesi. The nonlinear gyro-kinetic flux tube code GKW. *Computer Physics Communications*, 180(12):2650 – 2672, 2009. 40 years of CPC: A celebratory issue focused on quality software for high performance, grid and novel computing architectures.

[58] A. Bortolon, B. P. Duval, A. Pochelon, and A. Scarabosio. Observation of spontaneous toroidal rotation inversion in Ohmically heated tokamak plasmas. *Phys. Rev. Lett.*, 97:235003, Dec 2006.

[59] J. E. Rice, A. C. Ince-Cushman, M. L. Reinke, Y. Podpaly, M. J. Greenwald, B. LaBombard, and E. S. Marmar. Spontaneous core toroidal rotation in Alcator C-Mod L-mode, H-mode and ITB plasmas. *Plasma Physics and Controlled Fusion*, 50(12):124042, 2008.

[60] C. Angioni, R. M. McDermott, F. J. Casson, E. Fable, A. Bottino, R. Dux, R. Fischer, Y. Podoba, T. Pütterich, F. Ryter, and E. Viezzer. Intrinsic toroidal rotation, density peaking, and turbulence regimes in the core of tokamak plasmas. *Phys. Rev. Lett.*, 107:215003, Nov 2011.

[61] Y. J. Shi, W. H. Ko, J. M. Kwon, P. H. Diamond, S. G. Lee, S. H. Ko, L. Wang, S. Yi, K. Ida, L. Terzolo, S. W. Yoon, K. D. Lee, J. H. Lee, U. N. Nam, Y. S. Bae, Y. K. Oh, J. G. Kwak, M. Bitter, K. Hill, O. D. Gurcan, and T. S. Hahm. ECH effects on toroidal rotation: KSTAR experiments, intrinsic torque modelling and gyrokinetic stability analyses. *Nuclear Fusion*, 53(11):113031, 2013.

[62] J. C. Hillesheim, F. I. Parra, M. Barnes, N. A. Crocker, H. Meyer, W. A. Peebles, R. Scannell, A. Thornton, and the MAST Team. Dependence of intrinsic rotation reversals on collisionality in MAST. *Nuclear Fusion*, 55(3):032003, 2015.

[63] G. D. Conway, C. Angioni, R. Dux, F. Ryter, A. G. Peeters, J. Schirmer, C. Troester, CFN Reflectometry Group, and the ASDEX Upgrade team. Observations on core turbulence transitions in ASDEX Upgrade using Doppler reflectometry. *Nuclear Fusion*, 46(9):S799, 2006.

[64] A. Lebschy, R. M. McDermott, C. Angioni, B. Geiger, M. Cavedon, G. D. Conway, R. Dux,

E. Fable, T. Happel, A. Kappatou, A. Medvedeva, T. Ptterich, D. Prisiazhniuk, F. Ryter, U. Stroth, E. Viezzer, and the ASDEX Upgrade Team. Measurement of the ExB velocity across the LOC-SOC transition. In P. Mantica, G. Giruzzi, M. Fajardo, T. Gans, S. Poedts, and Geneva) N. Vennekens (European Physical Society, editors, *Europhysics Conference Abstracts (CD-ROM, Proc. of the 43th EPS Conference on Plasma Physics, Leuven, Belgium, 2016)*, volume 40A (2016), 2016.

[65] E Fable, C Angioni, and O Sauter. The role of ion and electron electrostatic turbulence in characterizing stationary particle transport in the core of tokamak plasmas. *Plasma Physics and Controlled Fusion*, 52(1):015007, 2010.